Optics Letters

High-repetition-rate few-cycle green source generation for sub-optical-cycle two-color Yb laser synthesizers

YUZHE LIU,[1,2] YIFAN LIU,[1,2] HAO ZHOU,[1,2] AOKUN ZHANG,[1,2] SENCHI YANG,[1,2] AND SHAOBO FANG[1,2,*]

[1] Institute of Physics, Chinese Academy of Sciences, Beijing 100049, China
[2] University of Chinese Academy of Sciences, Beijing 100049, China
*shaobo.fang@iphy.ac.cn

Received 16 March 2026; revised 11 April 2026; accepted 18 April 2026; posted 21 April 2026; published 1 May 2026

High-repetition-rate sub-optical-cycle synthesis based on two-color Yb lasers requires few-cycle pulses from both the fundamental wave (FW) and its second harmonic (SH). Yet generating few-cycle SH pulses remains challenging. Here, we demonstrate a 3.1 W few-cycle green source at 50 kHz using a strategy that first compresses the FW pulses, followed by frequency doubling and subsequent post-compression of the SH pulses in an argon-filled gas cell. The system derived pulses of 6.3 fs with 62-μJ pulse energy with 0.3% RMS power stability over 6 h, enabling strong-field electron dynamics control within sub-cycle regime and its applications at high signal-to-noise ratio.

https://doi.org/10.1364/OL.599102

Synthesizing a fundamental wave (FW) with its second harmonic (SH) breaks the temporal symmetry of the electric field. The resulting two-color asymmetric waveform enhances strong-field electron dynamics, e.g., tunnel ionization at favorable phases, increases the kinetic energy gained by electrons in the continuum, and modifies their return dynamics [1–3]. Compared with multi-channel synthesis based on a shared supercontinuum originating from the FW [4,5], two-color synthesis using the FW and its SH provides greater flexibility in controlling the relative phase and intensity ratio, thereby enabling more versatile manipulation of electron trajectories, quantum-path interference, and phase matching [6]. Recently, two-color synthesizer gain increasing importance for efficient high-harmonic generation [7,8] and terahertz emission [9,10]. Further compressing the FW and its SH both into few-cycle regime enables tailored sub-cycle electric field for precisely coherent control of electron dynamics in atomic, molecular, and solid-state systems [11,12].

To date, two-color configurations delivering few-cycle FW and SH pulses have merely been realized by kHz-level lasers [13–15]. For applications such as pump–probe spectroscopy [16] and angle-resolved photoemission spectroscopy [17], 100 kHz-level two-color few-cycle sources are highly desirable to achieve a high signal-to-noise ratio and more efficient data acquisition. Based on high-repetition-rate, Ytterbium laser offers an alternative, as few-cycle FW has been demonstrated through extensive spectral broadening and efficient compression [18–21]. However, compressing SH pulses further into the few-cycle regime remains challenging because of the lower damage threshold of the nonlinear media for stable spectral broadening and the more demanding dispersion management required for efficient pulse compression compared with the FW [22].

The conventional strategy places a frequency-doubling crystal directly after the Yb-laser output to generate near-200-fs SH pulses with high conversion efficiency, followed by post-compression to achieve sub-20-fs pulse duration [23–26]. However, a moderate SH conversion efficiency is more favorable for preserving the residual FW, thereby facilitating its recycling and compression for subsequent two-color synthesis [27]. To overcome these challenges, we propose a practical approach for generating a high-repetition-rate two-color few-cycle source from a Yb-based laser (Fig. 1). The strategy consists of three key ingredients:

1) Efficiently compress the Yb-laser output to 21.7 fs while maintaining high throughput using an optimized multi-pass-cell compressor (MPC).

2) Generate SH pulses directly after the MPC output with moderate conversion efficiency, resulting in 17.3-fs SH pulses and the 16-fs residual FW (FW1) while preserving sufficient energy and compressibility in both channels.

3) Further broaden the spectra of both the FW and SH pulses via gas-filled single-pass cell and subsequently compress them to the few-cycle regime.

Beyond demonstrating high-power, single-cycle FW through a cascaded MPC and single-pass scheme [28], this Letter presents a high-performance, two-color pulse compression architecture featuring a 6.3-fs SH output. In the initial stage, a high-efficiency MPC-based compressor reduces the pulse duration of a 400-μJ, 50-kHz Yb-laser from 180 fs to 21.7 fs while maintaining an exceptional energy throughput exceeding 97%. Subsequent SH generation yields 88-μJ, 17.3-fs green pulses; notably, this process simultaneously shortens the residual FW

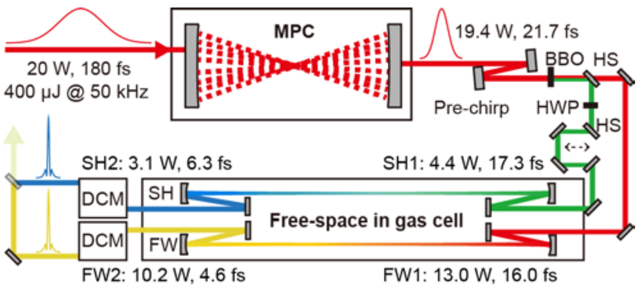

Fig. 1. Schematic diagram of the experimental setup. The phase-locking modules are currently under development (combination stage, indicated by the semi-transparent sections). DCM, double chirped mirror; HS, harmonic separator; HWP, half-wave plate.

from 21.7 fs to 16 fs. Furthermore, the residual FW is compressed to 4.6 fs (FW2). By focusing the SH pulses into an argon-filled gas cell for further spectral broadening, we achieved a supercontinuum spanning from 350 nm to 620 nm (at the −30 dB level). These broadened pulses were compressed to 6.3 fs with a pulse energy of 62 μJ, utilizing only group delay dispersion (GDD) compensation. The compressed pulses are near the transform-limit (TL) duration of 4.6 fs, achieving a total compression efficiency of over 70%. Approximately 60.4% of the pulse energy is contained within the main lobe, resulting in a peak power of 5.9 GW. Furthermore, the system exhibits excellent long-term robustness, with power fluctuations of less than 0.3% (RMS) over a 6-hour period.

Our experimental setup consists of an MPC for FW compression and a gas cell for two-channel pulse compression separately (Fig. 1). The details of the MPC configuration are provided in [28]. Following the MPC, a set of chirped mirrors is employed to introduce a pre-chirp of -200 fs^2 (Layertec GmbH, -100 fs^2 per bounce over the 950–1120 nm range). Subsequent SH pulses are generated using a 0.2-mm anti-reflection-coated (AR-coated) beta-barium borate (BBO) crystal, which is cut at 23.4° along the S-polarization direction. Two harmonics separators (HS) (Layertec GmbH, high reflectance at 480–550 nm, high transmittance at 925–1150 nm) and an achromatic half-wave plate (HWP) are used to filter the FW to a level of −50 dB, as verified by an optical spectrum analyzer (OSA, AQ6374E, Yokogawa), and rotate the SH pulses to P-polarization. To broaden the spectrum of SH pulses, a single-pass configuration is applied with pulses focused in an argon-filled gas cell (2 m × 0.3 m × 0.3 m). The collimated beam is compressed by two sets of customized DCMs (Ultrafast Innovations GmbH, −30 fs² per bounce at 350 – 700 nm with reflectivity >96%) and 20 cm of air for dispersion fine-tuning.

The temporal and spectral characteristics of the FW1 following the SH process were characterized using a SPIDER (FC SPIDER IR, APE GmbH). To isolate FW, an HS was placed before the characterization stage (Fig. 1), yielding an average power of 13.0 W. The FW1 duration was measured at 16.0 fs (Fig. 2(a)), which is notably shorter than the 21.7-fs pulses initially output from the MPC. This temporal profile corresponds to an energy fraction of 70% within the main lobe, resulting in a peak power of 11.4 GW. The broadened spectrum spans from approximately 900 nm to 1200 nm (Fig. 2(b)). The shortening of the FW is attributed to a combination of nonlinear spectral broadening within the BBO crystal and subsequent spectral shaping. Specifically, the BBO crystal was slightly detuned to

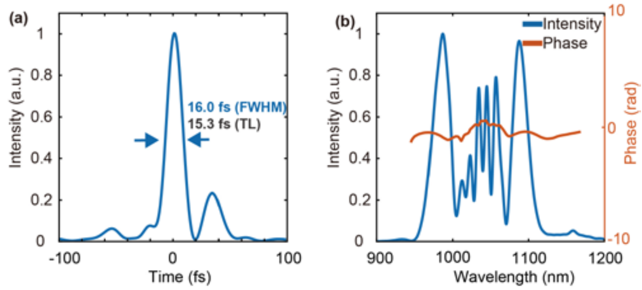

Fig. 2. Characterization of FW1 after HS. (a) Temporal intensity (blue line) along with the transform limit. (b) Retrieved spectral intensity (blue line) and phases (orange line).

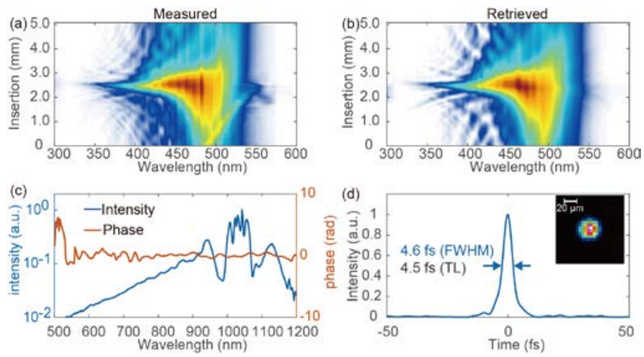

Fig. 3. Characterization of FW2. (a) Measured and (b) retrieved D-scan trance. (c) Spectral intensity (blue line) and the corresponding phase (red line). (d) Temporal intensity. Inset figure: far-field beam profile.

maximize SH conversion efficiency. In this configuration, the optimum phase-matching wavelength is located above 1070 nm, which reduces the spectral weight of longer wavelengths and induces a blue-shift of the center wavelength. The FW1 is focused into the argon-filled gas cell, yielding 4.6-fs pulses (TL: 4.5 fs) corresponding to 1.4 optical cycles, with more than 90.5% of the peak power concentrated in the main pulse (Fig. 3). The average output power is 10.2 W, corresponding to a peak power of 40.2 GW and an overall efficiency of 78%, the compressor and temporal characterization methods is detailed in [28]. The far-field beam profile, measured to be 35 μm in 1/e² diameter at the focus using a 50-mm off-axis parabolic mirror, corresponds to a peak intensity of approximately 8.3 PW/cm².

The average power of the SH pulses following two HS was measured at 4.4 W, corresponding to a conversion efficiency of 22.6%. The temporal and spectral characteristics of the SH pulses were characterized using a transient-grating frequency-resolved optical gating (TG-FROG) system. The TG signal was captured by a CMOS-based spectrometer (YIXIST, YSM-8106), while the reference spectrum was recorded using an OSA. The reconstructed TG-FROG trace (Fig. 4(b)) achieved a low retrieval error of 0.004 compared to the measured trace (Fig. 4(a)). The SH pulse duration was determined to be 17.3 fs, closely approaching the transform-limited (TL) duration of 16.5 fs (Fig. 4(c)). A comparison between the retrieved and measured spectra is provided in Fig. 4(d), revealing a slight residual high-order dispersion that is induced during the SH generation process. This temporal profile features an energy fraction of 83.8% within the main lobe, resulting in a peak power of 4.3 GW.

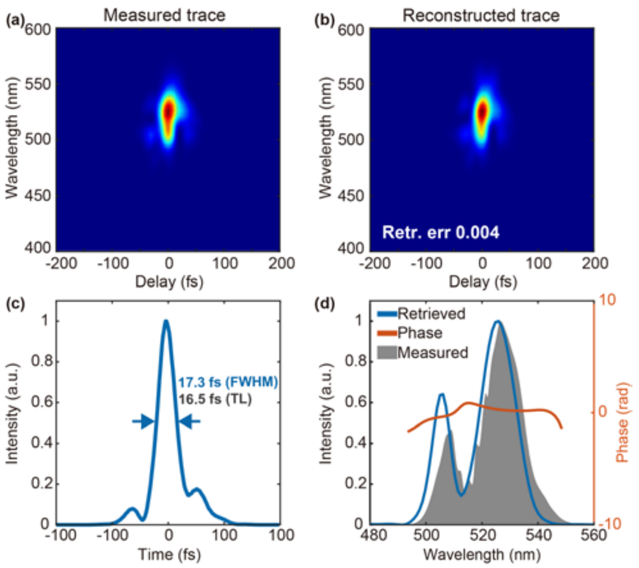

Fig. 4. Characterization of SH pulses after HS. (a) Measured and (b) reconstructed FROG trace. (c) Temporal intensity (blue line) along with transform limit. (d) Retrieved spectral intensity (blue line), phases (orange line), and measured spectral intensity (gray shadow).

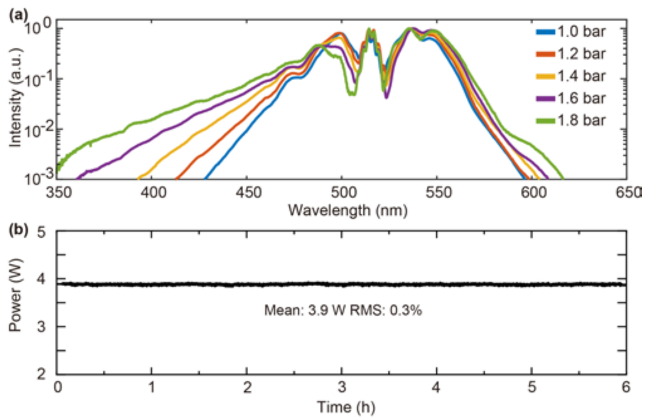

Fig. 5. (a) Pressure-dependent spectral broadening in an argon-filled gas cell. (b) Power stability of uncompressed output pulses after gas cell for over 6 hours.

The spectral broadening in the single-pass gas cell is finely adjusted by tuning the filled argon pressure from 1.0 bar to 2.0 bar, where the critical power P_{crit} varied from 3.6 GW to 1.8 GW, where the propagation length of the self-focusing beam until collapse L_c is rather well approximated by a semi-empirical formula:

$$L_c = \frac{0.367 L_{DF}}{\sqrt{\left[(P_{in}/P_{cr})^{1/2} - 0.852\right]^2 - 0.0219}}, \tag{1}$$

where P_{in} is the peak power of the input pulses, and L_{DF} is the Rayleigh length of the beam. Utilizing a focusing mirror with a 1500 mm radius of curvature for free-space propagation within the gas cell, the Rayleigh length is estimated to be ~5 mm. This yields a collapse length L_c varied from ~9.6 mm to 2.7 mm. Since L_c is comparable to or shorter than the Rayleigh length, it indicates that self-focusing and subsequent ionization occur during propagation.

The evolution of the SH spectrum was recorded using an OSA at 0.2-bar intervals, ranging from 1.0 bar to 1.8 bar (Fig. 5(a)). As the gas pressure increases, the spectrum broadens significantly; notably, the extension on the short-wavelength side is more pronounced than on the long-wavelength side. This asymmetry indicates that the spectral broadening is driven by a combination of self-phase modulation, self-steepening, and ionization-induced frequency blue-shifting effects. Spectral broadening begins to saturate at an argon pressure of 1.8 bar, with no further significant extension observed at 2.0 bar and 2.2 bar. Further increases in pressure led to degradation of both transmission efficiency and long-term stability. To maintain a stable output, the pressure was optimized at 1.6 bar, yielding a green-pulse supercontinuum spanning 350–620 nm (at the −30 dB level). The average power was measured at 3.9 W before the compression stage, with a long-term stability of 0.3% (RMS) over 6 hours (Fig. 5(b)). This minor degradation in stability, compared to the FW, is attributed to the nonlinear amplification of power and pointing jitters during the SHG process, which is highly sensitive to both input intensity and the angle of incidence.

To better verify the ionization behavior, simulations were performed by solving the unidirectional pulse propagation equation (UPPE) based on the numerical model reported in [29]. Assuming radially symmetric free-space propagation, the calculated beam radius at the focus is 88 μm. The discrepancy from the vacuum focusing condition indicates a non-negligible self-focusing effect within the Rayleigh length. Consequently, a weak ionization region is formed approximately 670–770 mm from the focusing mirror, corresponding to an advanced focal position relative to its vacuum focus. Using the Ammosov–Delone–Krainov (ADK) ionization model, the maximum ionization rate in this region is estimated to be 2.80×10^{-3} for argon at a pressure of 1.6 bar in the gas cell.

The average power following compression is 3.1 W, corresponding to an overall throughput efficiency of 70%. The primary energy losses are attributed to the silver-coated mirrors and the DCMs positioned after the gas cell. The temporal and spectral characteristics of the compressed SH pulses were also characterized using TG-FROG and an OSA, respectively. The reconstructed TG-FROG trace (Fig. 6(b)) exhibits a retrieval error of 0.007 relative to the measured trace (Fig. 6(a)), confirming a high-fidelity reconstruction. The compressed SH pulse duration was measured at 6.3 fs, corresponding to 3.7 optical cycles at the center wavelength with TL duration of 4.6 fs (Fig. 6(c)). This temporal profile features an energy fraction of 60.4% within the main lobe, resulting in a peak power of 5.9 GW. The far-field beam profile, measured to be 80 μm in $1/e^2$ diameter at the focus using a 50-mm off-axis parabolic mirror, corresponds to a peak intensity of approximately 0.2 PW/cm². This result confirms the high spatiotemporal quality required for strong-field applications under tight focusing. The oscillations observed in the retrieved spectral phase (Fig. 6(d)) are ascribed to the inherent trade-off between maximizing the effective bandwidth and achieving precise group delay dispersion (GDD) control during the DCM coating design process. Consequently, these residual phase fluctuations lead to the emergence of side lobes in the temporal profile. The compression results are summarized in Table 1. Here, FW1 and FW2 denote the residual FW after SH generation and the FW after the single-pass cell,

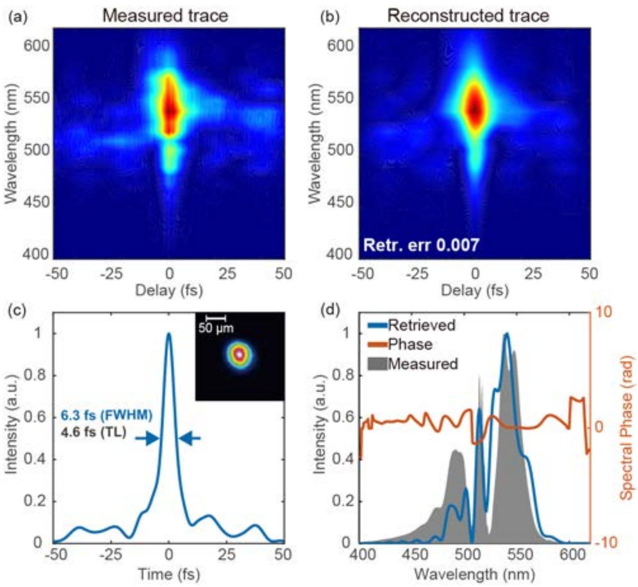

Fig. 6. Characterization of final compressed SH pulses. (a) Measured and (b) reconstructed FROG trace. (c) Temporal intensity (blue line) along with transform limit, inserted figure is the far-field beam profile. (d) Retrieved spectral intensity (blue line), phases (orange line), and measured spectral intensity.

Table 1. Summary of Compression Results

	Laser	MPC	FW 1	SH 1	FW 2	SH 2
Average power (W)	20	19.4	13.0	4.4	10.2	3.1
Pulse duration (fs)	180	21.7	16.0	17.3	4.6	6.3
Pulse energy (μJ)	400	388	260	88	204	62
Peak power (GW)	2.2	15.9	11.4	4.3	40.1	5.9

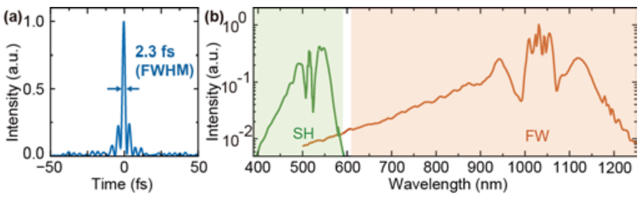

Fig. 7. Simulation of waveform synthesis using few-cycle SH and FW pulses. (a) Temporal synthesis of the FW and SH pulses. (b) Effective spectral ranges of the SH channel (green shading) and FW channel (orange shading) used for synthesis, together with their relative spectral intensities.

respectively, while SH1 and SH2 denote the SH pulses before and after the single-pass compressor, respectively.

In summary, we have demonstrated a high-power, two-color architecture capable of delivering 3.1-W, 62-μJ, 6.3-fs SH pulses at a 50-kHz repetition rate. The system exhibits exceptional long-term reliability, with a 6-hour power stability of better than 0.3% (RMS). Furthermore, we compressed the residual FW to 4.6 fs (1.4 cycle) via nonlinear process simultaneously.

We foresee that, with the active phase-locking modules currently being implemented based on our previous work [30] and the use of customized ultra-broadband dichroic mirrors optimized for both high spectral selectivity and dispersion control (Ultrafast Innovations GmbH, high reflectance at 350–590 nm, high transmittance at 610–1500 nm, both GDD optimized), this system provides a clear route toward controllable, high-power two-color synthesis. Simulations further indicate that combining the few-cycle SH pulses demonstrated here with a near-single-cycle FW can support 2.3-fs pulses, corresponding to 0.8 optical cycle at ~840 nm center wavelength (Fig. 7). We believe that such light source will serve as a powerful platform for efficient high-harmonic generation, broadband terahertz generation, and coherent control of attosecond electron dynamics.

Funding. Beijing Natural Science Foundation for Distinguished Young Scholars (JQ22015); Chinese Academy of Sciences Project for Young Scientists in Basic Research (YSBR-059); National Natural Science Foundation of China (U25A20515, 91950113, 61575219).

Acknowledgment. S. Fang gratefully acknowledges support from Professor Mikio Yamashita, Professor Franz X. Kaertner, and Synergetic Extreme Condition User Facility (SECUF-D5).

Disclosures. The authors declare no conflicts of interest.

Data availability. Data underlying the results presented in this paper are not publicly available at this time but may be obtained from the authors upon reasonable request.

REFERENCES

1. D. A. Telnov, J. Wang, and S.-I. Chu, Phys. Rev. A **52**, 3988 (1995).
2. I. J. Kim, C. M. Kim, H. T. Kim, *et al.*, Phys. Rev. Lett. **94**, 243901 (2005).
3. Z. Zeng, Y. Cheng, X. Song, *et al.*, Phys. Rev. Lett. **98**, 203901 (2007).
4. M. T. Hassan, T. T. Luu, A. Moulet, *et al.*, Nature **530**, 66 (2016).
5. Z. Pi, H. Y. Kim, and E. Goulielmakis, Optica **12**, 296 (2025).
6. L. Brugnera, D. J. Hoffmann, T. Siegel, *et al.*, Phys. Rev. Lett. **107**, 153902 (2011).
7. Y. Su, S. Fang, S. Wang, *et al.*, Appl. Phys. Lett. **120**, 121105 (2022).
8. A. Gindl, P. Suthar, F. Trojánek, *et al.*, Phys. Rev. Lett. **134**, 176903 (2025).
9. J. Zhao, J. Yang, X. Li, *et al.*, ACS Photonics **12**, 2034 (2025).
10. J. Buldt, H. Stark, M. Müller, *et al.*, Opt. Lett. **46**, 5256 (2021).
11. C. Heide, P. D. Keathley, and M. F. Kling, Nat. Rev. Phys. **6**, 648 (2024).
12. C. Manzoni, O. D. Mücke, G. Cirmi, *et al.*, Laser Photonics Rev. **9**, 129 (2015).
13. Y. Su, S. Fang, Y. Gao, *et al.*, Appl. Phys. Lett. **118**, 261102 (2021).
14. H.-T. Chang, M. Zürch, P. M. Kraus, *et al.*, Opt. Lett. **41**, 5365 (2016).
15. Y. Xia, P. Huang, T. Feng, *et al.*, Opt. Lett. **50**, 6253 (2025).
16. J. Li, Q. Ji, R. Wang, *et al.*, J. Am. Chem. Soc. **146**, 20312 (2024).
17. J. Wang, F. Chen, M. Pan, *et al.*, Opt. Express **31**, 9854 (2023).
18. Y. Liu, Z. Chen, S. Yang, *et al.*, Opt. Lett. **49**, 6992 (2024).
19. Y. Liu, Q. Chen, Y. Liu, *et al.*, APL Photonics **10**, 081301 (2025).
20. S. Goncharov, K. Fritsch, and O. Pronin, Opt. Lett. **48**, 147 (2023).
21. A.-L. Viotti, C. Li, G. Arisholm, *et al.*, Opt. Lett. **48**, 984 (2023).
22. S.-H. Chia, G. Cirmi, S. Fang, *et al.*, Optica **1**, 315 (2014).
23. M. Karst, P. Pfaller, R. Klas, *et al.*, Opt. Lett. **48**, 1300 (2023).
24. D. Descamps, F. Guichard, S. Petit, *et al.*, Opt. Lett. **46**, 1804 (2021).
25. V. Hariton, A. Bin Wahid, G. Figueira, *et al.*, Opt. Lett. **47**, 1246 (2022).
26. R. Klas, A. Kirsche, M. Gebhardt, *et al.*, PhotoniX **2**, 4 (2021).
27. J. Zhang, J. Y. Huang, H. Wang, *et al.*, J. Opt. Soc. Am. B **15**, 200 (1998).
28. Y. Liu and S. Fang, Opt. Lett. **50**, 5482 (2025).
29. C. Brahms and J. C. Travers, “Luna.jl: A flexible nonlinear optical pulse propagator,” https://github.com/LupoLab/Luna.jl.
30. P. Huang, S. Fang, Y. Gao, *et al.*, Appl. Phys. Lett. **115**, 031102 (2019).